General Disclaimer

One or more of the Following Statements may affect this Document

- This document has been reproduced from the best copy furnished by the organizational source. It is being released in the interest of making available as much information as possible.

- This document may contain data, which exceeds the sheet parameters. It was furnished in this condition by the organizational source and is the best copy available.

- This document may contain tone-on-tone or color graphs, charts and/or pictures, which have been reproduced in black and white.

- This document is paginated as submitted by the original source.

- Portions of this document are not fully legible due to the historical nature of some of the material. However, it is the best reproduction available from the original submission.

Produced by the NASA Center for Aerospace Information (CASI)

X-911-75-72
PREPRINT

NASA TM X-70904

A SATELLITE TECHNIQUE FOR QUANTITATIVELY MAPPING RAINFALL RATES OVER THE OCEANS

T. T. WILHEIT
M. S. V. RAO
T. C. CHANG
E. B. RODGERS
J. S. THEON

JUN 1975
RECEIVED
NASA STI FACILITY
INPUT BRANCH

MARCH 1975

GODDARD SPACE FLIGHT CENTER
GREENBELT, MARYLAND

(NASA-TM-X-70904) A SATELLITE TECHNIQUE FOR QUANTITATIVELY MAPPING RAINFALL RATES OVER THE OCEANS (NASA) 30 p HC $3.75 CSCL 04B

N75-25407

Unclas
G3/47 25998

CONTENTS

	Page
Abstract	v
Introduction	1
The ESMR System	3
Nimbus-5 Observations	10
Ground Based Verification	12
Conclusions	14
Acknowledgments	15
References	16

ILLUSTRATIONS

Figure		Page
1	Volume scattering coefficient and volume extinction coefficient at $\lambda = 1.55$ cm for a Marshall-Palmer distribution of raindrops at the indicated rain rate. The solid lines are based on an assumption of 20°C and the dashed lines are based on 0°C for the temperature of the raindrops	20
2	Relative, azimuthally averaged, angular distribution of scattering of 1.55 cm radiation by a Marshall-Palmer distribution of raindrops at 1 mm hr^{-1} (inner curve) and 25 mm hr^{-1} (outer curve). The two curves are not to the same scale	21
3	Calculated brightness temperature at 1.55 cm as a function of rain rate for freezing levels of 1, 2, 3, 4, and 5 km	22
4	Calculated brightness temperature at 1.55 cm as a function of rain rate with scattering included in the model (solid line) and excluded from the model (dashed line). In both cases, the assumed freezing level is 4 km	23

Figure		Page
5	A portion of the WSR-57 radar data for the June 25, 1973 case. The cross hatching shows the range and azimuth resolution of the radar. Isopleths of 0, 5, 10, and 50 mm hr^{-1} rain rate are indicated. The crosses (+) indicate the locations of the beam centers of the corresponding Nimbus-5 ESMR data. The 1.5 dB (inner oval) and 3 dB (outer oval) contour are shown for a typical ESMR beam position	24
6	Brightness Temperature as a function of rain rate: • Nimbus-5 ESMR vs. WSR-57 Radar + Inferred from ground based measurements of brightness temperature and direct measurements of rain rate. The solid line is the calculated brightness temperature for a 4 km freezing level. The dashed lines represent a departure of 2 mm hr^{-1} or a factor of two in rain rate (whichever is greater) from the calculated curve	25
7	Brightness temperature λ = 1.55 cm at a viewing angle of 45 degrees with respect to the zenith as a function of directly measured rain rate. At each point, the height and width of the cross represent two standard deviations in the corresponding dimensions. The solid line is the theoretically calculated curve	26
8	Brightness temperature λ = 0.81 cm at a viewing angle of 45 degrees with respect to the zenith as a function of directly measured rain rate. At each point, the height and width of the cross represent two standard deviations in the corresponding dimensions. The solid line is the theoretically calculated curve	27

Tables

Table		Page
1	Times and Dates of the WSR-57 Radar Observations	28
2	Radiometer Parameters	28

A Satellite Technique for Quantitatively Mapping

Rainfall Rates over the Oceans

by

T. T. Wilheit, M. S. V. Rao, T. C. Chang,

E. B. Rodgers, and J. S. Theon

Abstract

A theoretical model for calculating microwave radiative transfer in raining atmospheres is developed. These calculations are compared with microwave brightness temperatures at a wavelength of 1.55 cm measured by the Electrically Scanning Microwave Radiometer (ESMR) on the Nimbus-5 satellite and rain rates derived from WSR-57 meteorological radar measurements. A specially designed ground based verification experiment was also performed wherein upward viewing microwave brightness temperature measurements at wavelengths of 1.55 cm and 0.81 cm were compared with directly measured rain rates. It is shown that over ocean areas, brightness temperature measurements from ESMR may be interpreted in terms of rain rate with a minimum accuracy of a factor of two over the range 2 to 25 mm hr^{-1} rain rate.

Introduction

Since man's survival virtually depends upon favorable rainfall for the production of food, rainfall is one of the most widely observed meteorological parameters. Dating from the time of the earliest weather records, the measurement of rainfall over land surfaces has been a primary meteorological observation since this measurement requires only simple instrumentation. However, rainfall can be a sharply discontinuous process so that the rainfall measured at a point in space may not necessarily be representative of the larger scale rainfall pattern.

Perhaps even more important is the fact that the rainfall occurring over the oceans, which cover three-fourths of the Earth's surface, is very poorly known. Ship observations, as is well known, are unsatisfactory owing to platform instability and sea-spray problems. Island reports are not representative of the surrounding ocean because (a) there are vast oceanic areas where there are few islands and (b) even in regions with a fair number of islands, orographic effects modify the flow and rainfall patterns, especially in the tropics.

Radar has, to a limited degree, provided some insight into the complex nature of rainfall structure and variability. The advantage of radar, unlike the point measurements of a raingauge network, results from its ability to sense a volume of the atmosphere and translate this into rainfall rates over a given location. Serious problems with attenuation and calibration limit the accuracy of radar for the determination of rainfall, and its fixed location and limited

coverage make it unsuitable for global-scale measurements over the oceans. Thus, our knowledge of the total global rainfall and the water budget of the atmosphere is extremely limited. Whether the total rainfall under normal, drought, and wet years for a given geographical region is merely the result of redistribution of the rainfall, or the result of fluctuations in the global rainfall, or both, has been impossible to determine.

Many ingenious schemes for indirect estimation of rainfall have been devised, some of which may be mentioned. Barrett (1970) worked out a rainfall coefficient based on cloud cover and cloud type. Follansbee (1973) modified Barrett's areal statistics technique, concentrating upon rain-producing clouds (Cb, Ns and Cu congestus) to the exclusion of others. Another approach that has been developed relies upon the relationship between the reflected solar brightness of satellite pictures and rainfall rates. Martin and Suomi (1971, 1972) found that brightness regions correlate well with large radar echoes. Similarly, Woodley, Sancho, and Miller, (1972) concluded that the relationship of brightness area with precipitation depends upon whether the cloud system is young and vigorous, or old and decaying. (It is also worthwhile to remember that the brightness enhancement technique suffers from the dependence of brightness on sun angle and viewing geometry as well as from signal saturation and sensor degradation.) In the infrared techniques developed by Scherer and Hudlow (1971), cloud height and area derived from High Resolution Infrared Radiometer(HRIR) data were utilized to estimate precipitation, cirrus contamination

being ignored. Another indirect method adopted by Tucker (1961), and followed by Reed and Elliott (1973) to estimate precipitation in the northern Pacific, involves developing quantitative relations between current weather (ww) and rainfall amounts (RR) in the present weather reports from land stations and extending these relations to infer rainfall from ship weather reports.

The Electrically Scanning Microwave Radiometer (ESMR) system provides a more nearly direct approach. The greatest advantage of the system (which will be outlined in brief presently) is its selective response to liquid water. Although admittedly there are certain limitations, ESMR seems to be a better tool than any other available at present.

The ESMR System

The ESMR System carried on Nimbus 5 (Wilheit 1972; Wilheit, et al., 1973) receives radiation emitted by the earth and its atmosphere in a band of width 250 MHz centered at 19.35 GHz. The antenna beam scans perpendicular to the direction of satellite motion in an arc of 100 degrees every 4 secs, the resolution being a 25 km circle near nadir degrading to an oval 45 km downtrack × 160 km cross track at the ends of the scan. The brightness temperature as observed from the satellite is dependent upon the emission from the earth's surface modified by the intervening atmosphere. The emissivity, being a function of the dielectric constant, is variable over land surfaces (depending on vegetation, soil type, etc.) and generally large (ca. 0.9), but over oceans, the

emissivity is more or less uniform at the ESMR wavelength (1.55 cm) and has a low value (ca. 0.4). Furthermore, at the ESMR frequency, emissivity of water (ϵ_w) varies almost inversely as its thermodynamic temperature (T_w), with the result that the brightness temperature ($\epsilon_w T_w$) of a smooth water surface is virtually independent of temperature. Salinity has no consequential effect on the 19.35 GHz radiance from the surface of the ocean. The wind at the surface of the ocean does affect the emissivity (Nordberg et al, 1971; Hollinger, 1971). However, this effect is not strong enough to be a significant source of error in the present context.

It has been shown that the ESMR data may be qualitatively interpreted as indicating the presence or absence of rain above an unspecified threshold intensity (Wilheit, et al, 1973), and that the rain rate could be at least crudely estimated (Allison et al, 1974). This qualitative relationship between ESMR brightness temperature and rainfall has been exploited by Allison, et al (1975) in a study of tropical cyclones. In the present paper, this relationship will be established on a quantitative basis, theoretically supported, and independently confirmed.

The equation of radiative transfer (Chandrashekar 1960) may be written:

$$\frac{dT_B(\theta)}{dz} + \gamma_{ext} T_B(\theta) = \gamma_{sca} \int_0^{\pi} T_B(\theta_s)\, F(\theta, \theta_s) \sin\theta_s d\theta_s + \gamma_{abs} T(z)$$

for an axially symmetric distribution of the γ's and T, an axially symmetric scattering process, and using the Rayleigh-Jeans approximation. Here $T_B(\theta)$ is the radiance in the direction specified by the polar angle (θ) expressed as an equivalent blackbody temperature or brightness temperature. The coordinate z is distance along a ray path, θ_s the scattering angle, γ_{ext} the total attenuation due to scattering and absorption, γ_{sca} the scattering coefficient, and γ_{abs} the absorptivity. $F(\theta, \theta_s)$ is the angular distribution of the scattering integrated azimuthally and normalized to 1; T(z) is the thermodynamic temperature of the absorbing medium. Physically, the first term on the left hand side of the equation expresses the change in the radiance in a particular direction. The second term (γ_{ext} $T_B(\theta)$) gives the contribution to this change due to both absorption and scattering away from the specified angle. The integral term on the right hand side expresses the increase in radiance in the θ direction due to scattering from other angles, and the last term (γ_{abs} T(z)) represents the thermal emission of the medium.

In an atmosphere with rain, three constituents contribute significantly to the absorption: molecular oxygen, water vapor, and liquid water droplets. At these frequencies, ice crystals are essentially transparent. Water droplets are the sole source of scattering of microwave radiation considered here. The oxygen contribution consists of a large number of resonances between 50 and 70 GHz which blend into a continuum at sea level pressures and a single isolated line at 118.7 GHz. The effect at the frequencies considered here (19.35 and 37.0 Hz)

is only about 2K; the model used is that of Meeks and Lilley (1963) as modified by Lenoir (1968). The effect of water vapor is due to a weak resonance at 22.235 GHz and a number of strong ones at 183 GHz and higher frequencies. The model for the absorption coefficient of water vapor used here is that given by Staelin (1966).

The interaction of a dielectric sphere with a plane electromagnetic wave was first solved by Mie (1908), and was discussed in the context of clouds and rain droplets by Gunn and East (1954). The extinction (absorption and scattering) cross section of a liquid water droplet is given by:

$$\sigma_{ext} = -\frac{\lambda^2}{2\pi} \mathrm{Re} \sum_{n=1}^{\infty} (2n+1)(a_n + b_n)$$

and the scattering cross section by:

$$\sigma_{sca} = \frac{\lambda^2}{2\pi} \sum_{n=1}^{\infty} (2n+1)(|a_n|^2 + |b_n|^2)$$

where the magnetic and electric 2^n pole coefficients a_n and b_n are from expressions given by Stratton (1956) using the dielectric data of Lane and Saxton (1952). The angular distribution of amplitude of the scattered electromagnetic radiation is the sum of the radiation from the magnetic and electric 2^n poles. In the limit of small droplet, of radius less than about 100 μm for the frequencies considered here, only the electric dipole term b_1 need be considered. In this case the scattering is insignificant and the extinction cross section, which is then equivalent to the absorption cross section, reduces to:

$$\sigma_{abs} = \sigma_{ext} = \frac{4\pi^2\rho^3}{\lambda} \operatorname{Im}\left\{\frac{1-k}{2+k}\right\}$$

where ρ is the radius of the droplet and k is the dielectric constant of water at the appropriate frequency. The absorption cross section is thus proportional to the volume of the droplet. The absorptivity can be related to the absorption cross section of a single droplet by:

$$\gamma_{abs} = \int N(\rho)\, \sigma_{abs}(\rho)\, d\rho$$

where $N(\rho)$ is the number density per unit size interval of droplets of radius ρ. Thus, the absorptivity is proportional to the mass density of the water droplet distribution, independent of the droplet size distribution as long as there are no particles with radius greater than about 100 μ m. This condition is quite valid for non-raining clouds. The distribution of precipitating particles in a rainstorm is given by the Marshall-Palmer distribution:

$$N(\rho) = N_0 e^{-81.56\,\rho R^{-0.21}}$$

where $N(\rho)$ is the number density of particles per unit size interval, ρ is in cm, R is the rain rate in millimeters per hour, and the proportionality constant N_0 has the value $8 \times 10^{-2} cm^{-4}$ for any intensity of rainfall. This distribution was derived from physical measurements on rain drops at the surface and has been found to predict the radar returns from rain storms fairly well (Marshall, et al, 1947; Marshall and Palmer, 1948).

When the scattering and extinction cross sections with the dielectric properties appropriate for a frequency of 19.35 GHz and temperatures of 273K and 293K are numerically integrated over the Marshall-Palmer distribution, the coefficients of extinction and scattering shown in Figure 1 result. In Figure 2, the azimuthally averaged relative angular distributions of the scattering are shown for rain rates of 1 mm hr^{-1} and 25 mm hr^{-1}. In the low rain rate case, the droplets scatter like electric dipoles oriented in the direction of the incoming electric field vector; thus the forward and backward scattering components are roughly equal and twice as large as the scattering perpendicular to the direction of incidence. In the 25 mm hr^{-1} case, the larger particle size permits other multipole components to contribute, and the backward scattering is much larger than the forward scattering due primarily to interference between the electric and magnetic dipole components.

For purposes of calculation, the atmosphere is divided into many optically thin layers. A Marshall-Palmer distribution of rain droplets and 100% relative humidity are assumed from the freezing level to the surface. Since the Marshall-Palmer distribution does not include the cloud water droplets, a cloud with a net density of 25 mg cm^{-2} is distributed through the 1/2 km beneath the freezing level. The ocean surface is assumed to have the reflectivity given by the Fresnel relations (Jackson 1962), based on the Lane and Saxton (1952) dielectric data. A lapse rate of 6.5°C km^{-1} is assumed and the surface temperature (or equivalently, freezing level) is adjusted as a parameter of the calculation. Above the freezing

level, the relative humidity given by the 1962 U. S. Standard Atmosphere for that altitude is assumed. Water droplets are described by the using of Lane and Saxton (1952) dielectric data. The angular distribution of reflection from the ocean surface is assumed to be Lambertian (Peake et al, 1966).

Using this model, the up-and-downwelling brightness temperatures are then computed, first ignoring the scattering so that the brightness temperatures may be computed for a number of angles independently. The brightness temperatures are then recomputed iteratively using the brightness temperatures of the previous iteration for the scattering term until satisfactory convergence (to better than 1K) is obtained.

Brightness temperatures for a set of five atmospheres and a range of rainfall rates were calculated for a frequency of 19.35 GHz. The surface temperatures were 279.6, 286.1, 292.6, 299.1, and 305.6K, giving freezing levels of 1, 2, 3, 4, and 5 km, respectively. The Marshall-Palmer distribution of rain particles appropriate to each rain rate was assumed from the freezing level to the surface. The results of this calculation are shown in Figure 3. Note that there is no consequential effect of rain at rates less than 1 mm hr^{-1}, but above that, the brightness temperature increases sharply with increasing rain rate to a maximum of about 255K around 50 mm hr^{-1} rain rate. At higher rain rates, the very strong backscattering of the larger droplets actually decreases the brightness temperature. The dependence on freezing level is about 50% in rain rate per km change in the freezing level at a given brightness temperature.

To demonstrate the effect of scattering, the brightness temperatures were calculated for the 4 km freezing level case with the scattering term artificially suppressed in the calculation. The results of this calculation are compared to the full calculation in Figure 4. Up to 10 mm hr^{-1}, there is little effect due to the scattering, but above this value, the effect is to significantly lower the brightness temperature and to cause a maximum to appear in the brightness temperature calculated with scattering, whereas the no-scattering case approaches 273K asymptotically.

Nimbus-5 Observations

To confirm this theoretical model, simultaneous measurements of rain rate and microwave brightness temperature over ocean areas were needed. Four cases were found where data were taken by the WSR-57 meteorological radar at Miami, Florida coincident with Nimbus-5 overpasses (to within 5 minutes). The dates and times of these are given in Table I. In all cases, a tropical maritime atmosphere with the freezing level at 4 km was assumed.

The WSR-57 meteorological radar measures the backscattered microwave signal at a wavelength of 10.3 cm (2.91 GHz). The range resolution is 1.2 km out to a maximum of 120 km. The azimuthal resolution is 2 degrees. The return signal in each range-azimuth bin is digitally converted to rain rate through a statistically derived relationship; this rain rate is expressed in tenths of millimeters per hour. Further description of the WSR-57 radar and

the means by which radar return may be interpreted as rain rate can be found in Wiggert and Ostlund (1975).

In order to compare the data, the WSR-57 data were first plotted on a map base; the ESMR data were then overlaid using the image of the Florida coast line and Lake Okeechobee visible in the ESMR data as a guide to insure registration. Figure 5 is an image of the WSR-57 data for the pass, the crosses (+) show the location of the beam centers for the corresponding ESMR data. The two ovals show the approximate 3 dB (half power) and 1.5 dB antenna gain contours for a typical ESMR beam position. Since the ESMR resolution is much coarser than that of the WSR-57, the radar data must be averaged over the radiometer resolution element. To approximate the effect of the antenna pattern, the radar data within the 1.5 dB gain contour were given full weight while those between the 1.5 dB and 3.0 dB contours were given half weight in the averaging. Only those beam positions with centers more than 50 km from the coast and with scan angles of less than 40 degrees were included. The greatest rain rate observed was 79 mm hr^{-1} in the June 25, 1974 case. However when averaged to the ESMR resolution, the maximum observed was 16.6 mm hr^{-1}. In Figure 6, the results of this comparison are shown as solid points. The solid line is the brightness temperature computed for the 4 km freezing level. The two dashed lines represent departures of the larger of a factor of two in rain rate or 2 mm hr^{-1}. Note that virtually all the points are within or very near this envelope. The crosses (+) are inferred from the ground based measurements discussed in the next section.

Ground Based Verification

As further verification of the theoretical model, two microwave radiometers with center frequencies of 19.35 and 37.0 GHz were mounted viewing upward at a 45 degree zenith angle. The relevant parameters of each are summarized in Table 2. The rectangular cross section, horn-type antennas were mounted with the electric field vector horizontal so that the E-plane antenna gain pattern, having larger sidelobes than the H-plane gain pattern, caused a minimum variation in elevation throughout the field of view. The antenna horns were shielded from direct rain by a wooden housing open on one side. They were protected against wetting from blowing rain by using a plastic wrapping across their apertures and a blower which directed a stream of dry air across the plastic wrap. The receivers were connected in turn for a period of 15 seconds each (a) to their respective antennas, (b) to a reference cold load, and (c) to a reference warm load. The output from this radiometer system was fed to a small computer which calculated both of the mean brightness temperatures for the 15 seconds when the radiometers were sensing the radiation from the antennas (separately at 19.35 and 37.0 GHz) and printed out the results at intervals of 0.8 minutes.

Two rain gauges of different types were used to measure the rainfall intensities simultaneously with the radiometer observations. The first was a conventional tipping bucket rain gauge located adjacent to the antenna housings. The number of times the bucket tipped was registered by a counter and recorded on the computer print-out alongside the radiometer readings. The second was

the recently developed (Raymond and Wilson, 1974) electronic rain intensity gauge with a 1 second response time, located at a horizontal distance of 23.5 meters away from the radiometers in the direction of the antenna beams. In this type of rain gauge, measurement is made of the ratio of the resistance of rain water flowing in a trough between two electrodes spaced along the trough (R_1), to the resistance of the same rain water in a chamber of fixed geometry (R_2). Since R_1 varies as the resistivity divided by the cross sectional area of the flowing water while R_2 varies only as the resistivity, R_2/R_1 is independent of resistivity and is proportional to the cross section area, i.e., it is related only to the rate of flow. Both rain gauges were calibrated against directly measured flow rates and both had 91 cm funnel apertures.

Data were collected with this arrangement from June through September 1974, at Goddard Space Flight Center. On all occasions on which data were taken, the freezing level was 4 ± 0.5 km. With the aid of the laboratory calibration curve, the voltage records on chart paper were translated to rainfall rates. The brightness temperatures of the 19.35 and 37.0 GHz radiometer systems were tabulated against rainfall intensities. For this purpose, only those occasions when the rain rate and temperatures were sensibly steady for two minutes or more were considered, in order to avoid excessive scatter in the data. The observations were then grouped under 18 categories according to rainfall rate intervals (10 categories at 1 mm hr^{-1} intervals from 0 to 10 mm hr^{-1}, 5 at 2 mm hr^{-1} intervals from 10 to 20 mm hr^{-1}, 2 at 10 mm hr^{-1} intervals from 20 to 40 mm hr^{-1}, and

one final category greater than 40 mm hr^{-1}). In each category the mean and standard deviation were calculated separately with respect to brightness temperature ($\bar{T}_B$ and σ_{T_B}) and rainfall ($\bar{R}$ and σ_R). The diagram in Figure 7 shows the result for 19.35 GHz and the diagram in Figure 8 those for 37.0 GHz. In both diagrams, the vertical lines and horizontal lines are equal in length to 2 standard deviations. The solid curve, in each case, represents the corresponding theoretical calculation.

If one approximates the radiometric effect in this case by an isothermal, non-scattering layer of absorber at a temperature of 273K, these upward viewing data can be converted to what would have been observed by the ESMR if this atmosphere were over water. These data are included in Figure 6 and are quite consistent with the satellite observations and the theoretical calculations.

Conclusions

There are many weaknesses inherent to a study of this type. The most obvious is that there is much uncertainty in interpretation of radar returns in terms of rain rate. There is also some uncertainty in registering the ESMR data to the radar data; and having registered the two, it is not feasible to use an exact antenna pattern in averaging the rain rate over the instantaneous field of view of the ESMR. The non-linearity of the rain rate/brightness temperature relationship reduces the validity of such an average still further. There are other variable factors which have been ignored; water vapor, wind speed and

viewing angle, to name a few. All these factors contribute to the considerable scatter in the observed relationship between ESMR brightness and radar derived rain rates. Nevertheless, the data show clearly that in the dynamic range 2-20 mm hr^{-1} rain rate, brightness temperature at 19.35 GHz can be related to rain rate to within a factor of two. Considering the difficulty of any rain rate measurement over an area, this is quite a useful measurement. The upward viewing data agree well with the theoretical model over a wide range of rain rates and at two different frequencies (19.35 and 37 GHz) so that by using this model, the microwave response to rain may be predicted for other frequencies and viewing geometries. Since global data are now available from the Nimbus-5 ESMR, it is possible to measure the oceanic component of the atmospheric water budget.

Acknowledgments

The authors gratefully acknowledge the aid of Dr. W. L. Woodley and his coworkers at the Experimental Meteorological Laboratory, NOAA, Coral Gables, Florida, for the radar data; Dr. C. M. Fullerton of the Cloud Physics Laboratory, University of Hawaii, for the loan of the electronic rain gauge; Dr. R. J. Curran for the radiative transfer computer program, and Mr. A. E. Burbage for efforts much beyond his normal duties in operating the ground based verification experiment.

REFERENCES

Allison, L., E. Rodgers, T. Wilheit, and R. Wexler, 1975: "A Multi-Sensor Analysis of Nimbus-5 Data on 22 January 1973," NASA-TN-D-7911.

Allison, L., E. Rodgers, T. Wilheit, and R. Fett, 1974: "Tropical Cyclone Rainfall as Measured by the Nimbus-5 Electrically Scanning Microwave Radiometer," BULL. AMER. METEOR. SOC., 55, 9, 1074-1089.

Barrett, E. C., 1970: "The Estimation of Monthly Rainfall from Satellite Data," MON. WEA. REV., 98, 322-327.

Chandrashekar, S., 1960: "Radiative Transfer," NEW YORK, DOVER, INC.

Follansbee, W., 1973: "Estimation of Average Daily Rainfall from Satellite Cloud Photographs," NOAA TECH, MEMO., NESS 44, 39 pp.

Gunn, K. L. S. and T. U. R. East, 1954: "The Microwave Properties of Precipitation Particles," QUART. J. ROY. METEOR. SOC., 80, 522-545.

Hollinger, J. P., 1971: "Passive Microwave Measurements of Sea Surface Roughness," IEEE, TRANS. ON GEOSCIENCE ELECTRONICS, GE-9, No. 3, 165-169.

Jackson, J. D., 1962: "Classical Electrodynamics," WILEY & SONS, INC., NEW YORK, p 216 ff.

Lane, J. A. and J. A. Saxton, 1952: "Dielectric Dispersion in Pure Polar Liquids at Very High Radio Frequencies," PROC. ROY. SOC., LONDON A, 213, 400-408.

Lenoir, W. B., 1968: "Microwave Spectrum of Molecular Oxygen in the Mesosphere," J. GEOPHYSICAL RESEARCH, 73, 361-376.

Martin, D. W. and V. Soumi, 1971: "A Satellite Study of Cloud Clusters Over the Tropical North Atlantic Ocean," FINAL REPT. ON TASK ORDER 13, Space Science and Engineering Center, Madison, Wis., 80 pp.

Martin, D. W. and V. Soumi, 1972: "A Satellite Study of Cloud Clusters Over the Tropical North Atlantic Ocean," BULL. AMER. METEOR. SOC., 53, 135-156.

Marshall, T. S., R. C. Langille and W. McK. Palmer, 1947: "Measurement of Rainfall by Radar," J. MET. 4, 186-192.

Marshall, T. S. and W. McK. Palmer, 1948: "The Distribution of Raindrops with Size," J. MET. 5, 165-166.

Meeks, M. L. and A. Lilley, 1963: "The Microwave Spectrum of Oxygen in the Earth's Atmosphere," J. GEOPHYS. RES. 68, 6.

Mie, G., 1908: "Beiträge zur Optik trüber Medien, speziell kolloidaler Metallösungen," ANNALEN DER PHYSIK., 26, 597-614.

Nordberg, W., J. Conaway, D. Ross and T. Wilheit, 1971: "Measurement of Microwave Emission from a Foam-Covered Wind Driven Sea," J. ATMOS. SCI., 28, No. 3, 429-435.

Peake, W. H., R. Riegler and C. Shultz, 1966: "The Mutual Interpretation of Active and Passive Microwave Sensor Outputs," PROC. 4th SYMP. ON REMOTE SENSING OF ENVIRONMENT, Univ. Mich.

Raymond, D. J. and K. Wilson, 1974: "Development of a New Rainfall Intensity Gauge," J. APPLIED MET., 13, 180-182.

Reed, R. K. and W. P. Elliott, 1973: "Precipitation at Ocean Weather Stations in the North Pacific," J. GEOPHYS. RES., 78(30), 7087-7091.

Scherer, W. D. and M. Hudlow, 1971: "A Technique for Assessing Probable Distributions of Tropical Precipitation Echo Lengths for X-Band Radar from Nimbus 3 HRIR Data," BOMEX BULL. No. 10, NOAA, 63-68.

Staelin, D. A., 1966: "Measurements and Interpretation of the Microwave Spectrum of the Terrestrial Atmosphere Near 1 Centimeter Wavelength," J. GEOPHYS. RES., 71, 2875-2881.

Stratton, J. A., 1956: "Spheroidal Wave Functions, Including Tables of Separation Constants and Coefficients," Technology Press of MIT and WILEY & SONS, INC., NEW YORK.

Tucker, G. B., 1961: "Precipitation Over the North Atlantic Ocean," QUART. J. ROY. METEOR. SOC., 87, 147-158.

Wiggert V. and Ostlund, S., 1975: "Computerized Rain Assessment and Tracking of South Florida Weather Radar Echoes," BULL. AMER. METEOR. SOC, 56, 17-26.

Wilheit, T., 1972: "The Electrically Scanning Microwave Radiometer (ESMR) Experiment," Nimbus-5 User's Guide, NASA, Goddard Space Flight Center, Greenbelt, Maryland, 59-105.

Wilheit, T., J. Theon, W. Shenk, L. Allison and E. Rodgers, 1973: Meteorological Interpretations of the Images from Nimbus-5 Electrically Scanning Microwave Radiometer," NASA X-651-73-189, 21 pp. To be published in J. APP. MET.

Woodley, W. L., B. Sancho and A. Miller, 1972: "Rainfall Estimation from Satellite Cloud Photographs," NOAA TECH. MEMO. ERL-OD-11, 43 pp.

FIGURE CAPTIONS

Figure 1. Volume scattering coefficient and volume extinction coefficient at $\lambda = 1.55$ cm for a Marshall-Palmer distribution of raindrops at the indicated rain rate. The solid lines are based on an assumption of 20°C and the dashed lines are based on 0°C for the temperature of the raindrops.

Figure 2. Relative, azimuthally averaged, angular distribution of scattering of 1.55 cm radiation by a Marshall-Palmer distribution of raindrops at 1 mm hr^{-1} (inner curve) and 25 mm hr^{-1} (outer curve). The two curves are not to the same scale.

Figure 3. Calculated brightness temperature at 1.55 cm as a function of rain rate for freezing levels of 1, 2, 3, 4 and 5 km.

Figure 4. Calculated brightness temperature at 1.55 cm as a function of rain rate with scattering included in the model (solid line) and excluded from the model (dashed line). In both cases, the assumed freezing level is 4 km.

Figure 5. A portion of the WSR-57 radar data for the June 25, 1973 case. The cross hatching shows the range and azimuth resolution of the radar. Isopleths of 0, 5, 10, and 50 mm hr^{-1} rain rate are indicated. The crosses (+) indicate the locations of the beam centers of the corresponding Nimbus-5 ESMR data. The 1.5 dB (inner oval) and 3 db (outer oval) contour are shown for a typical ESMR beam position.

PRECEDING PAGE BLANK NOT FILMED

Figure 6. Brightness Temperature as a function of rain rate:

- ● Nimbus-5 ESMR vs. WSR-57 Radar
- + Inferred from ground based measurements of brightness temperature and direct measurements of rain rate.

The solid line is the calculated brightness temperature for a 4 km freezing level. The dashed lines represent departure of 2 mm hr^{-1} or a factor of two in rain rate (whichever is greater) from the calculated curve.

Figure 7. Brightness temperature λ = 1.55 cm at a viewing angle of 45 degrees with respect to the zenith as a function of directly measured rain rate. At each point, the height and width of the cross represent two standard deviations in the corresponding dimensions. The solid line is the theoretically calculated curve.

Figure 8. Brightness temperature λ = 0.81 cm at a viewing angle of 45 degrees with respect to the zenith as a function of directly measured rain rate. At each point, the height and width of the cross represent two standard deviations in the corresponding dimensions. The solid line is the theoretically calculated curve.

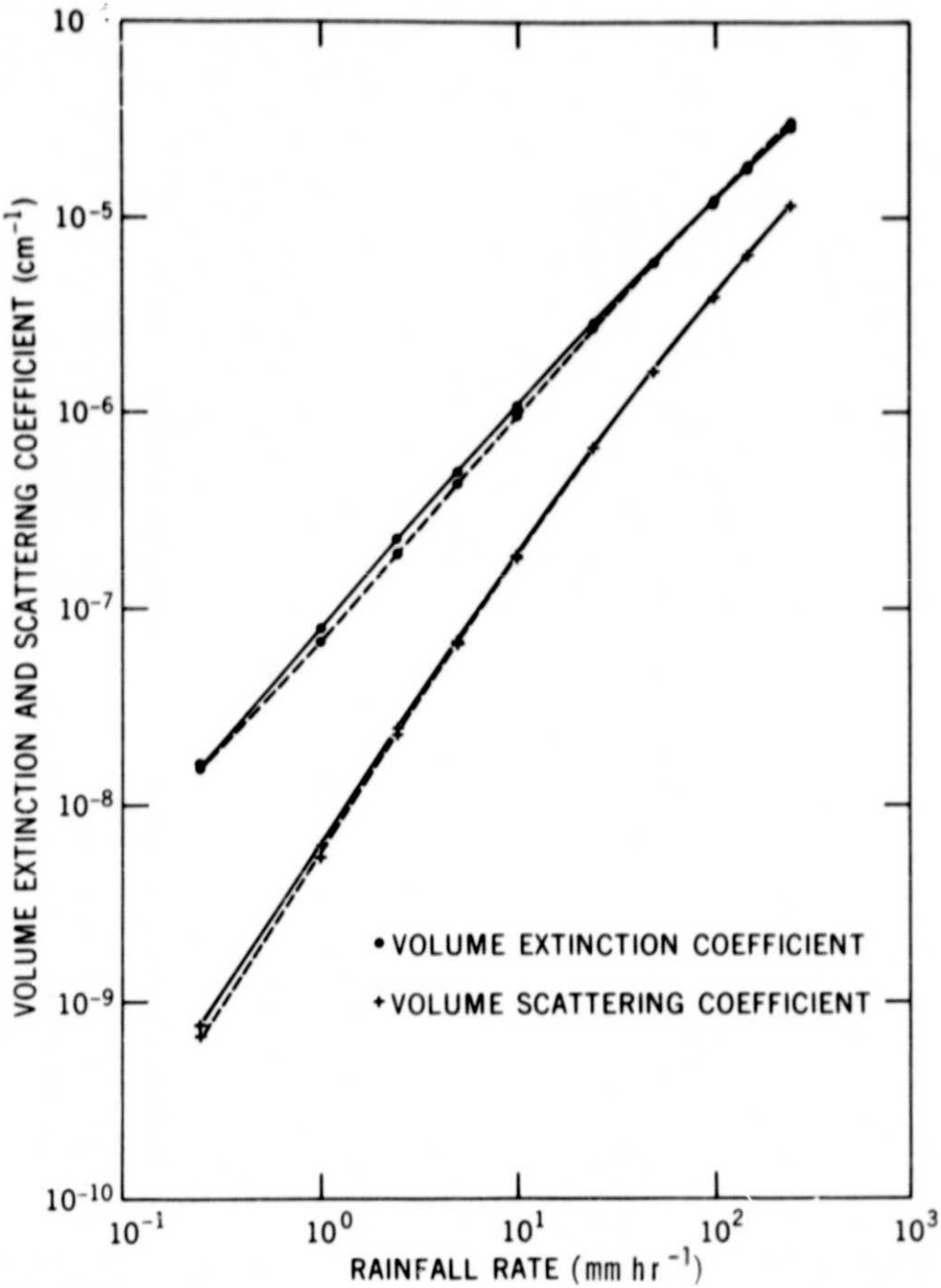

Figure 1. Volume scattering coefficient and volume extinction coefficient at $\lambda = 1.55$ cm for a Marshall-Palmer distribution of raindrops at the indicated rain rate. The solid lines are based on a assumption of 20°C and the dashed lines are based on 0°C for the temperature of the raindrops.

Duplicate page numbers

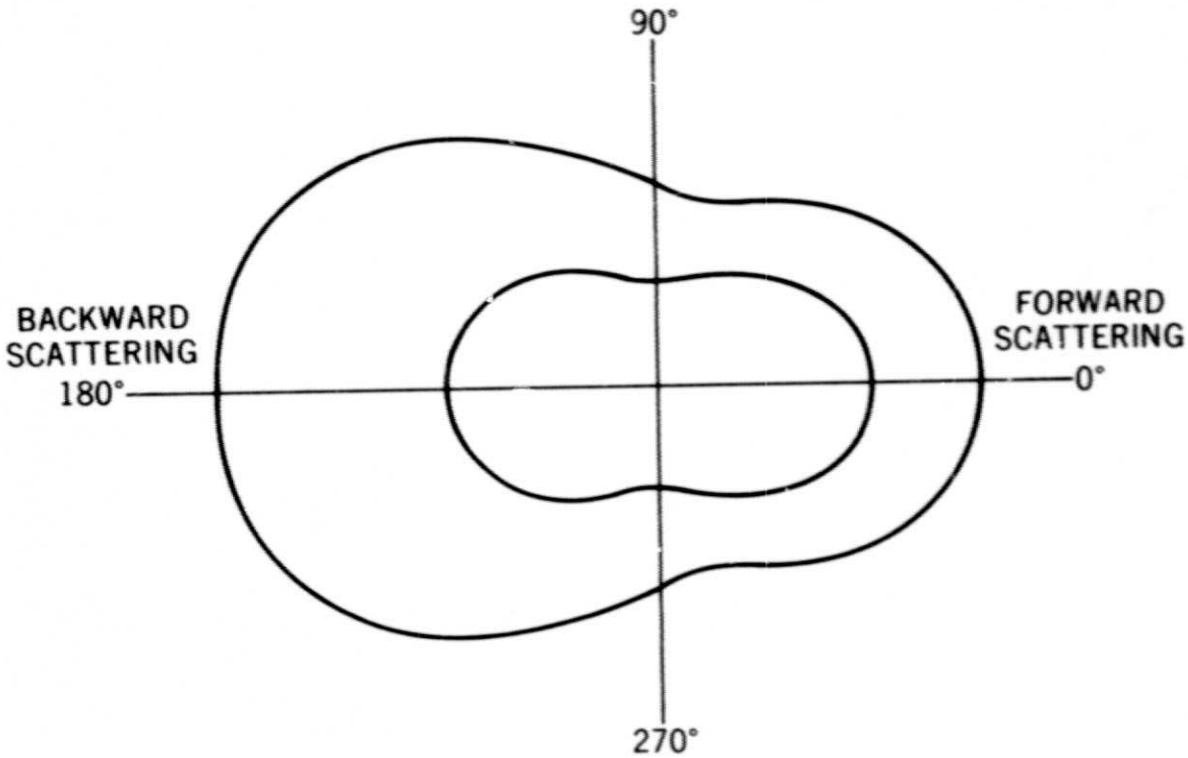

Figure 2. Relative, azimuthally averaged, angular distribution of scattering of 1.55 cm radiation by a Marshall-Palmer distribution of raindrops at 1 mm hr^{-1} (inner curve) and 25 mm hr^{-1} (outer curve). The two curves are not to the same scale.

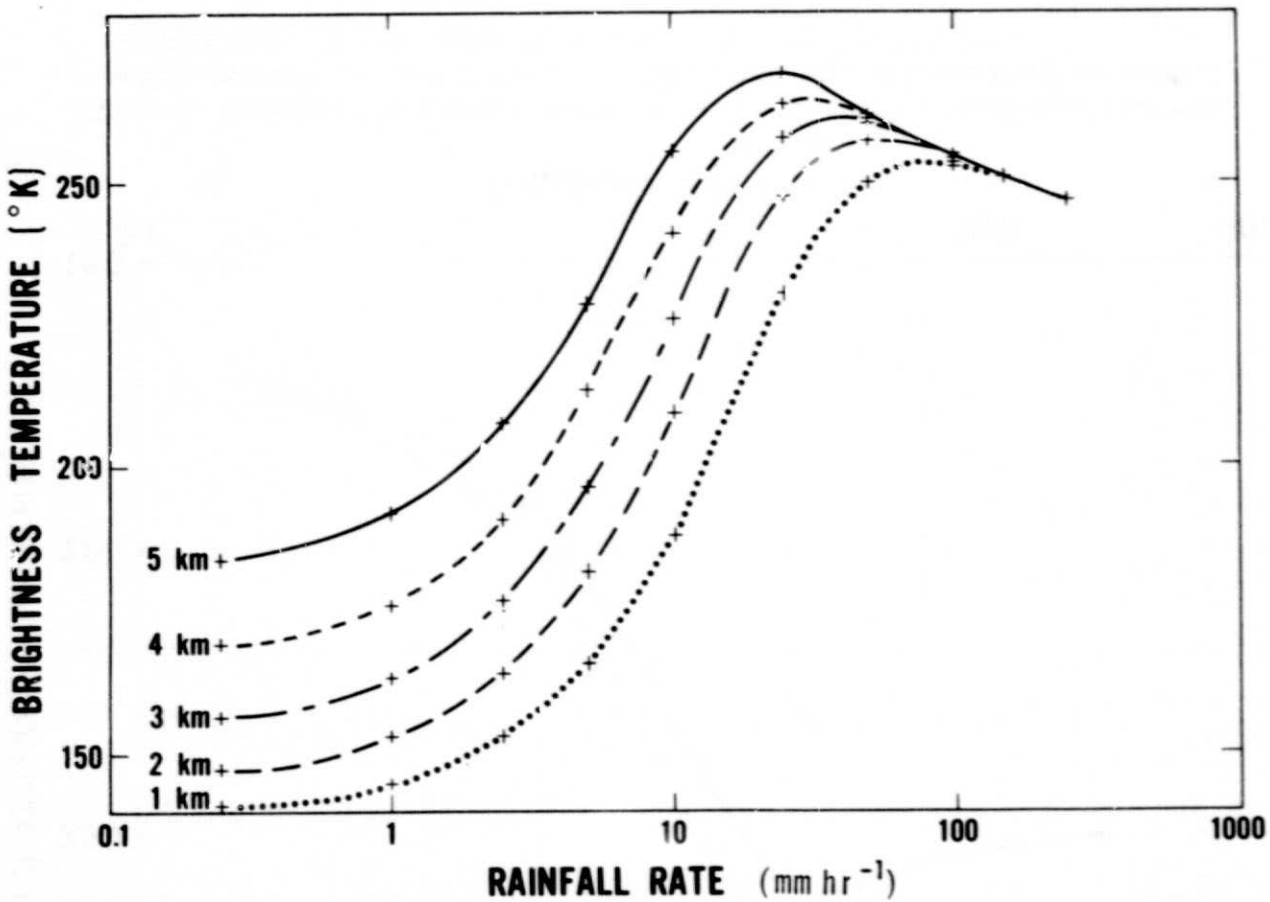

Figure 3. Calculated brightness temperature at 1.55 cm as a function of rain rate for freezing levels of 1, 2, 3, 4 and 5 km.

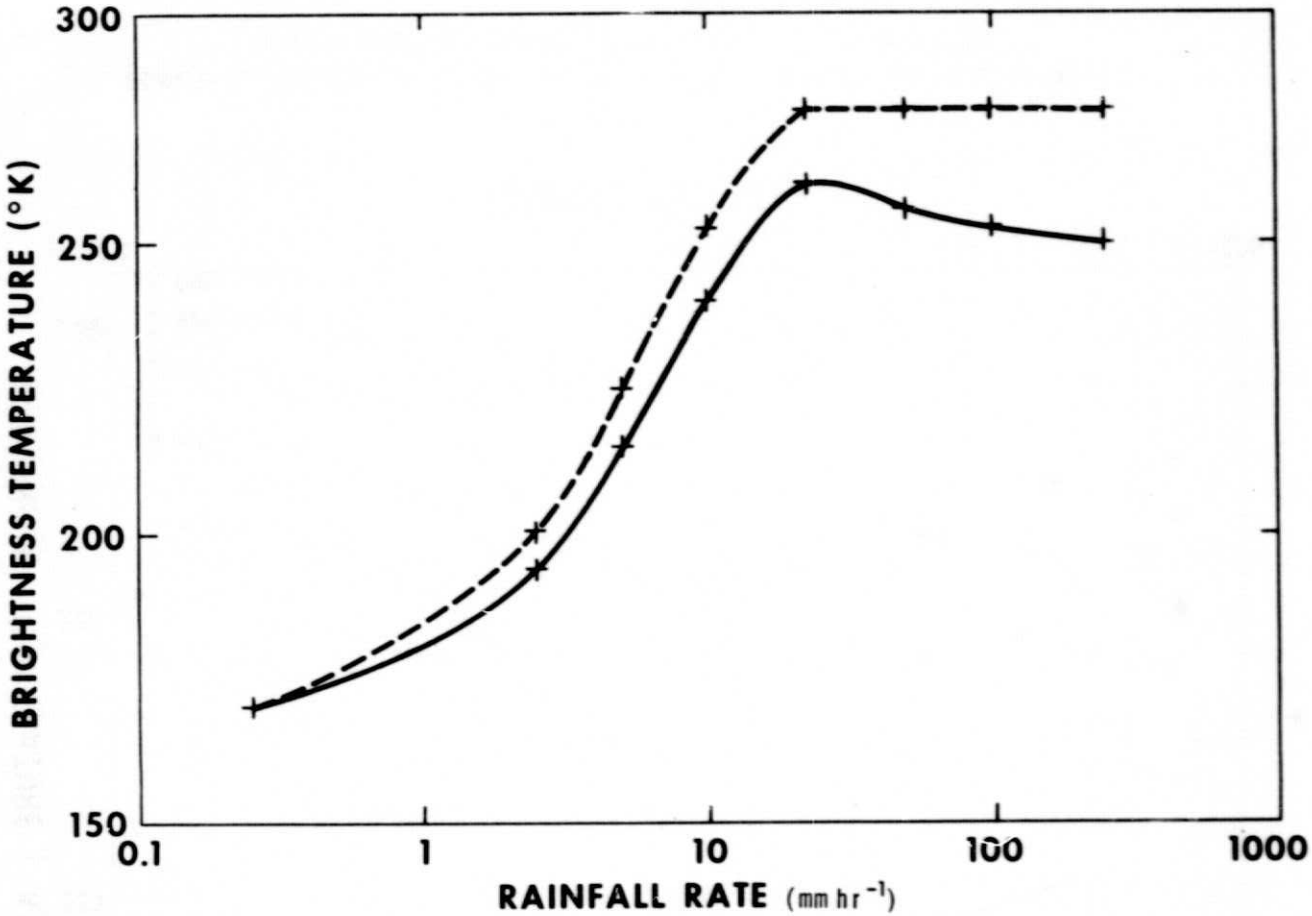

Figure 4. Calculated brightness temperature at 1.55 cm as a function of rain rate with scattering included in the model (solid line) and excluded from the model (dashed line). In both cases, the assumed freezing level is 4 km.

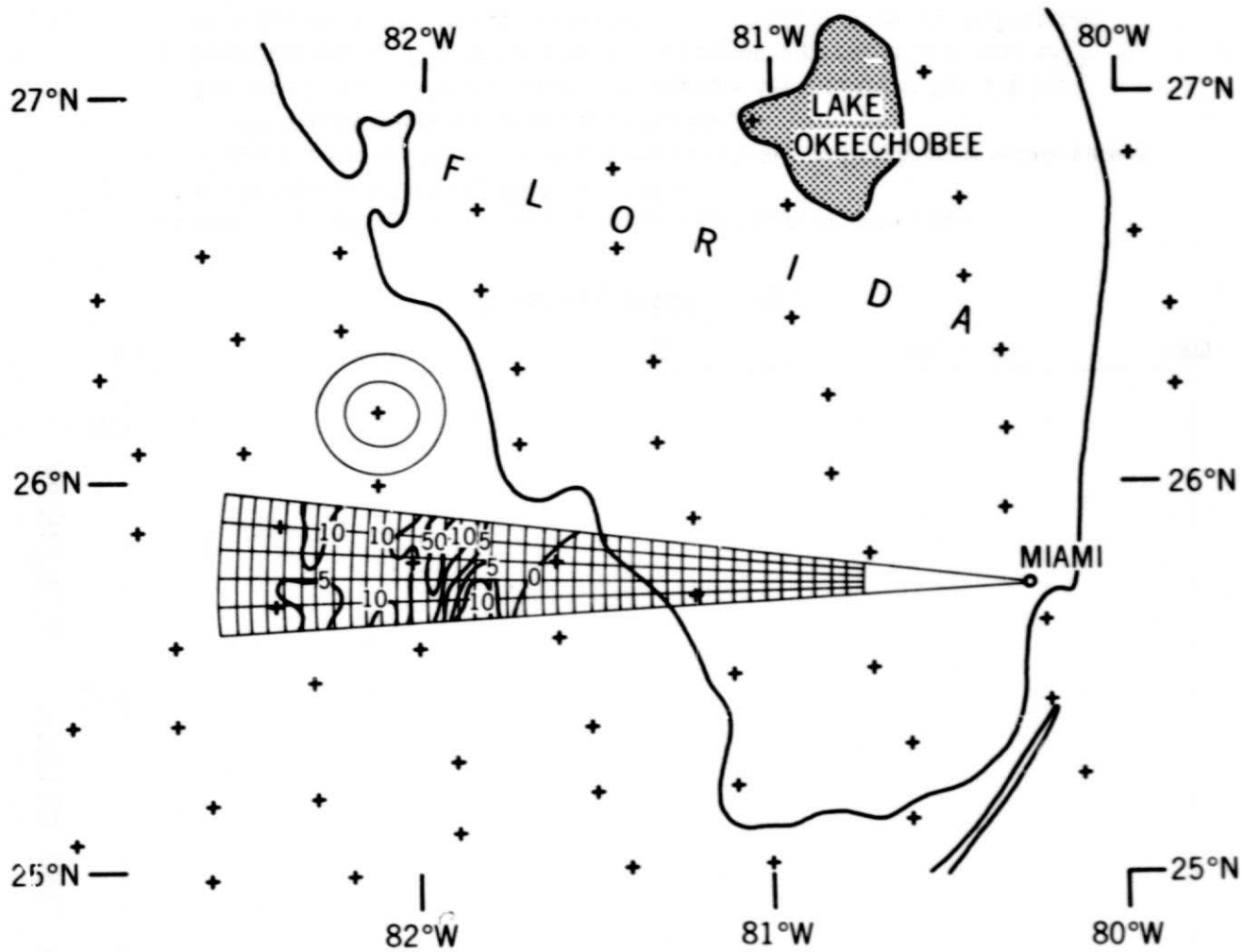

Figure 5. A portion of the WSR-57 radar data for the June 25, 1973 case. The cross hatching shows the range and azimuth resolution of the radar. Isopleths of 0, 5, 10, and 50 mm hr^{-1} rain rate are indicated. The crosses (+) indicate the locations of the beam centers of the corresponding Nimbus-5 ESMR data. The 1.5 dB (inner oval) and 3 dB (outer oval) contour are shown for a typical ESMR beam position.

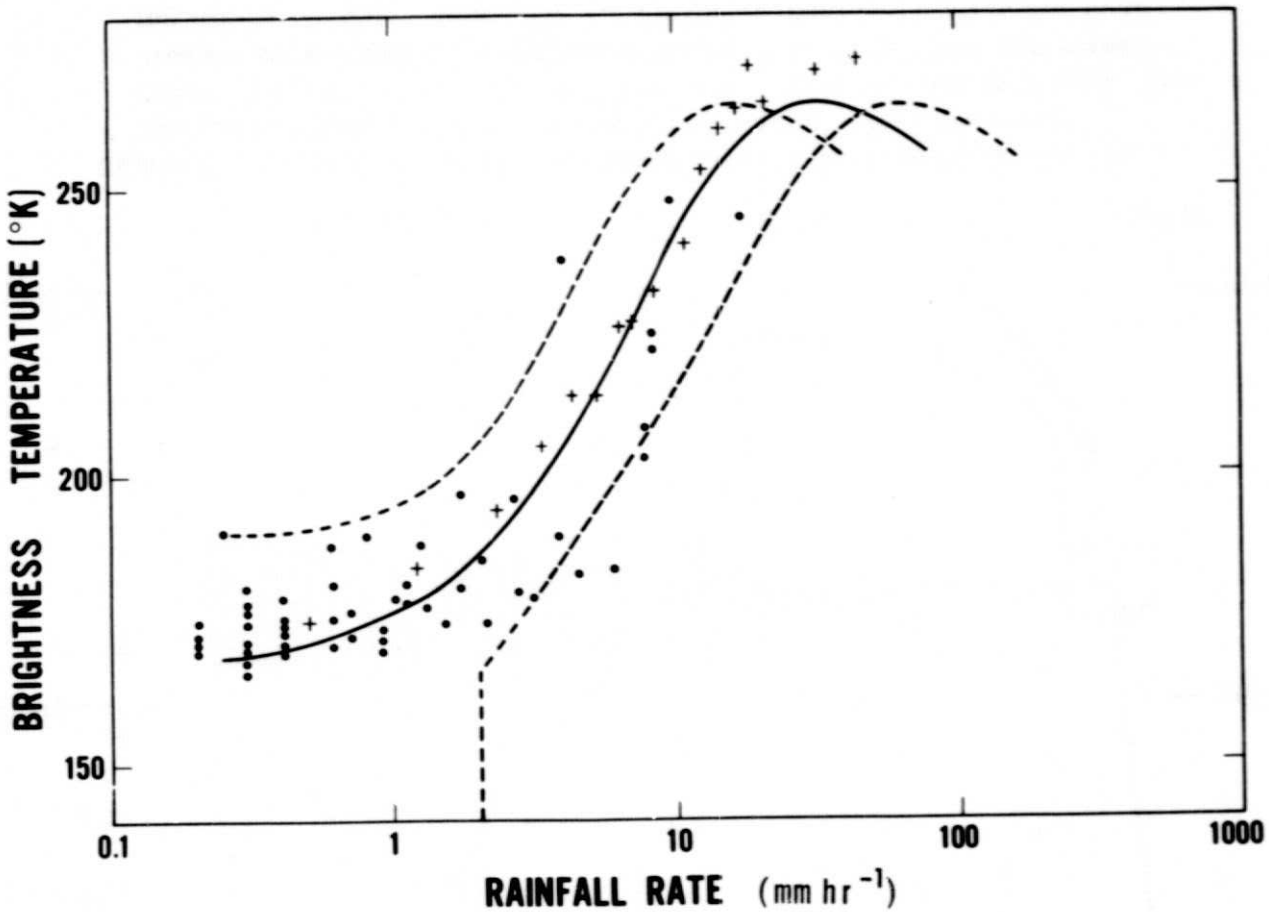

Figure 6. Brightness Temperature as a function of rain rate:

- ● Nimbus-5 ESMR vs. WSR-57 Radar
- + Inferred from ground based measurements of brightness temperature and direct measurements of rain rate.

The solid line is the calculated brightness temperature for a 4 km freezing level. The dashed lines represent departure of 2 mm hr^{-1} or a factor of two in rain (whichever is greater) from the calculated curve.

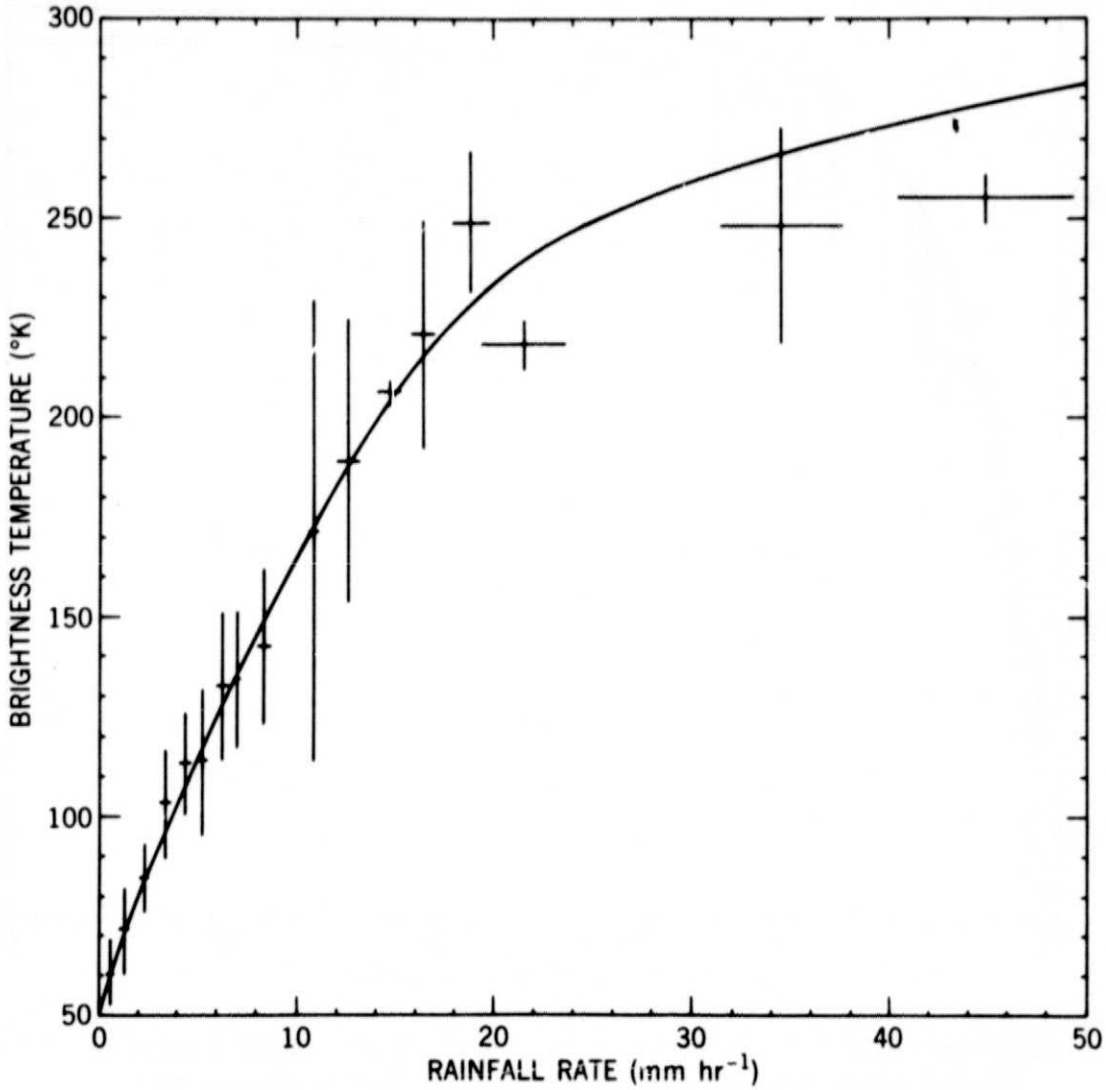

Figure 7. Brightness temperature λ = 1.55 cm at a viewing angle of 45 degrees with respect to the zenith as a function of directly measured rain rate. At each point, the height and width of the cross represent two standard deviations in the corresponding dimensions. The solid line is the theoretically calculated curve.

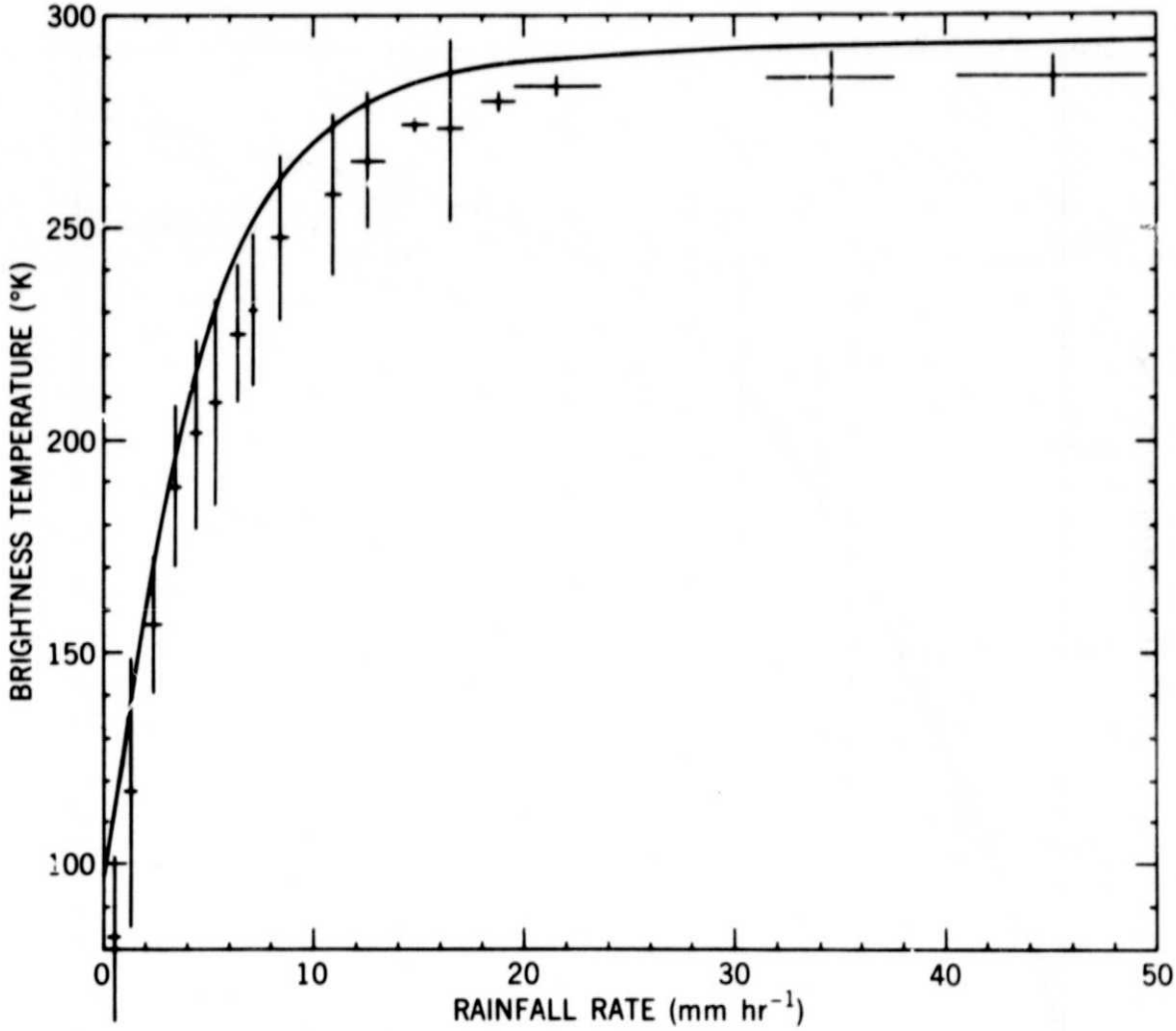

Figure 8. Brightness temperature $\lambda = 0.81$ cm at a viewing angle of 45 degrees with respect to the zenith as a function of directly measured rain rate. At each point, the height and width of the cross represent two standard deviations in the corresponding dimensions. The solid line is the theoretically calculated curve.

Table 1
Times and Dates of the WSR-57
Radar Observations

Date	Time
20 June 1973	1632 GMT
7 July 1973	1610 GMT
24 June 1974	1605 GMT
25 June 1974	1705 GMT

Table 2
Radiometer Parameters

	Radiometer 1	Radiometer 2
Frequency	19.35 GHz	37.0 GHz
Wavelength	1.55 cm	0.81 cm
Bandwidth	400 MHz	400 MHz
E plane Beamwidth	6.5 degrees	6.5 degrees
H plane Beamwidth	9.0 degrees	9.0 degrees